Journal of Inorganic and General Chemistry
ZAAC
Zeitschrift für anorganische und allgemeine Chemie
DOI: 10.1002/zaac.202000461
ARTICLE

Increasing the Activity of Copper Guanidine Quinoline Catalysts: Substitution at the Quinoline Backbone Leads to Highly Active Complexes for ATRP

Konstantin W. Kröckert,[a] Johannes S. Mannsperger,[a] Thomas Rösener,[a] Alexander Hoffmann,[a] and Sonja Herres-Pawlis*[a]

Dedicated to Professor Dr. Peter Klüfers on the Occasion of his 70th Birthday

Copper bromide complexes with the ligands TMG6NO_2qu, TMG6Brqu, TMG6Methoxyqu, TMG6NMe_2qu, TMG6EHOqu and TMG6dBAqu were examined regarding their activity in atom transfer radical polymerization (ATRP). The ligands were inspired by 1,1,3,3-tetramethyl-2-(quinolin-8-yl)guanidine (TMGqu) and the substituents have been chosen with a large range between electron withdrawing and donating abilities. The donor properties of the ligands can be strongly influenced and further highly active catalysts based on these systems can be obtained. The ligands with strong donating moieties were in addition modified by alkyl groups to increase the solubility in apolar monomers like styrene. Cu^{I} and Cu^{II} bromide complexes were crystallised and the structural data correlated to the different substituents and the catalyst activity. The electrochemical potentials $E_{1/2}$, the equilibrium constants K_{ATRP} and rate constants k_{act} and k_{deact} were determined. Polymerizations of styrene were conducted in solution whereas the catalyst based on TMG6EHOqu shows a good solubility and performance in bulk.

Introduction

Atom Transfer Radical Polymerization (ATRP) was developed in 1995 and has become one of the most widely used reversible-deactivation radical polymerization (RDRP) methods.[1] Numerous investigations on catalytic systems are still ongoing due to desired properties regarding controlled conditions, a high tolerance to air and the use of ppm levels of catalyst.[2] Scheme 1 shows the ATRP mechanism in which a transition metal complex mediates a reversible equilibrium between dormant species and active radicals as growing chains. The activator complex accepts a halogen atom from the dormant radical species and so free radicals are formed.[3] Termination reactions of the radicals are possible, but they are largely suppressed by small radical concentrations and the persistent radical effect (PRE).[4] Further, the free radicals can react with the monomer or reversibly react with the transition metal complex to the dormant species. Here a fast exchange between the polymer chains is the key for a controlled polymerization with narrow molar mass distributions.[5] The position of the equilibrium is described by the equilibrium constant (K_{ATRP}) which is defined as the ratio of the activation (k_{act}) and deactivation (k_{deact}) rate constants. In common ATRP the equilibrium lies on the dormant side to reduce the free radical concentration and enable controlled conditions. For polymerizations with lower catalyst loadings or to polymerise less active monomers higher values of K_{ATRP} are necessary.[6] The nature of the catalyst is one option to tune these properties. Copper based systems with N-donor ligands are the most intensively used ATRP catalysts. It was found that their activity is severely

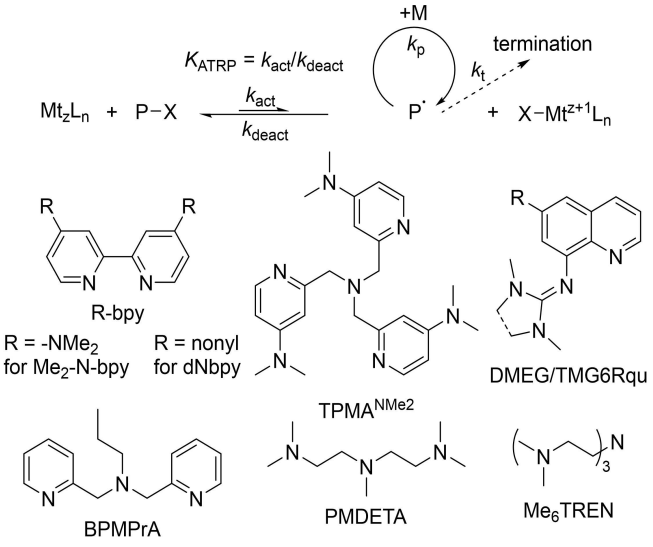

Scheme 1. ATRP equilibrium and investigated ligand systems.[7–10]

[a] *K. W. Kröckert, J. S. Mannsperger, T. Rösener, A. Hoffmann, S. Herres-Pawlis*
Institute of Inorganic Chemistry
RWTH Aachen University
Landoltweg 1A
52074 Aachen
E-mail: sonja.herres-pawlis@ac.rwth-aachen.de

Supporting information for this article is available on the WWW under https://doi.org/10.1002/zaac.202000461

affected by the nature of the N-donors, the electron donating properties and the denticity of the ligand.[7] Studies with 4,4′-substituted 2,2′-bipyridine ligands (left of Scheme 1) have shown that the electronical properties of an ATRP catalyst can be significantly influenced by electron donating and withdrawing groups. Here modifications with NMe_2 substituents exhibited the highest increase in activity.[8] The catalyst incorporating the $TPMA^{NMe2}$ ligand (middle of Scheme 1) is currently the most active system. Based on this tetrapodal ligand a K_{ATRP} value of around 1 is possible.[9]

Our group has its focus on guanidine ligands because they have excellent N-donor properties and several guanidine complexes show catalytical activity not just in ATRP[10–11] but also in ring-opening polymerization of lactide[12] or oxygen activation.[13] We showed already that copper catalysts of guanidine quinoline (GUAqu) ligands TMGqu and DMEGqu (right of Scheme 1, R = H) are highly active in ATRP reactions.[11a] Concerning to the redox potential they are comparable to catalysts like the tridentate PMDETA (bottom right of Scheme 1). Moreover this class of guanidine ligands exhibits remarkable reactivity in copper photochemistry[14] and as entatic state models for electron transfer proteins.[15] A problem for the ATRP was that unsubstituted copper halide GUAqu catalysts have a bad solubility in apolar monomers like styrene. So the first improvement was to modify the quinoline backbone with alkyl substituents (right of Scheme 1, R = Et, Bu) to increase the solubility.[10]

Besides optimising the ATRP performance of this system by better solubility, we demonstrate here that it is also possible to vary and enhance the activity by electronic effects. Substituents at the C6-position of the quinoline were varied by electron withdrawing (right of Scheme 1, R = NO_2, Br) and donating (R = OMe, NMe_2) groups with a large range of Hammett parameters.

In the present study, the successful modifications to change the solubility of guanidine quinoline systems were considered whilst introducing ethylhexyloxy (EHO) and dibutylamine (dBA) substituents. These alkyl chains should influence the polarity of the complexes beside pushing electron density into the system. Through more donating substituents, it was expected that the Cu^{II} species is more stabilized and larger ATRP constants obtained. The copper halide guanidine quinoline complexes were examined towards their molecular structures, redox potentials and activity in ATRP.

Results and Discussion

Synthesis of the Ligands

Here we present four novel guanidine quinoline ligands $TMG6NO_2qu$ (**L1**), $TMG6NMe_2qu$ (**L4**), TMG6EHOqu (**L5**) and TMG6dBAqu (**L6**). The ligands TMG6Brqu (**L2**) and TMG6Methoxyqu (**L3**) were synthesized according to the literature.[16] The guanidine synthesis of the ligands was accomplished according to a general procedure starting from amine precursors (Scheme 2).[17]

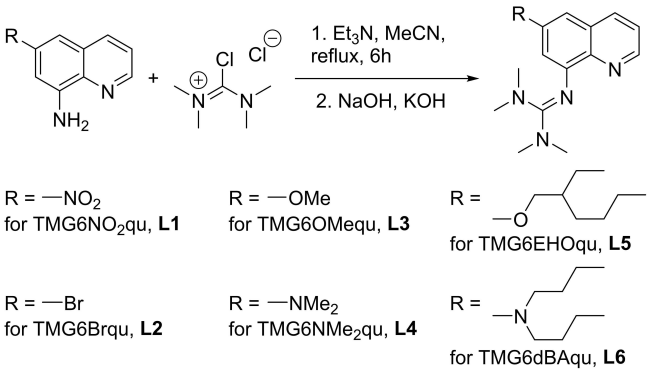

Scheme 2. Synthesis of differently substituted tetramethylguanidine quinoline ligands.

The preparation of each differently substituted ligand follows individual synthetic routes (Scheme 3). The precursor for ligand **L1** was synthesized according to Smalley *et al.*[18] For the precursor of ligand **L4**, N^1,N^1-dimethyl-3-nitrobenzene-1,4-diamine (**1**) was synthesized by an adjusted route related to literature.[19] The quinoline moiety was synthesized inspired by a protocol of Wielgosz-Collin *et al.*[20] Here compound **1** and acrolein (**2**) react to the substituted nitroquinoline **3** which then was reduced by sodium dithionite to the amine **4**. The synthesis of **L5** begins with the alkylation of 8-nitroquinolin-6-ol (**5**) by 3-(bromomethyl)heptane (**6**) analogue to Mewshaw *et al.* and Smil *et al.*[21] The nitro compound **7** was reduced in a Pd catalysed hydrogenation and yielded the amine **8**. The precursor of **L6** could be synthesized via a Buchwald-Hartwig amination from 6-bromo-8-nitroquinoline (**9**) to the nitro compound **11** and further the reduction to the amine **12**. Experimental details to all reactions can be found in the Supporting Information.

Synthesis and structural characterization of the copper guanidine complexes

The ligands (**L1**–**L4**) form copper guanidine quinoline complexes by a reaction with CuBr and $CuBr_2$. These were crystallized and examined by single crystal X-ray diffraction to investigate correlations between structural properties and the activity in ATRP with regard to the different substituents. The eight complexes $[Cu(TMG6NO_2qu)Br]$ (**C1-I**), $[Cu(TMG6NO_2qu)_2Br]Br \cdot CH_3CN$ (**C1-II**), [Cu(TMG6Brqu)Br] (**C2-I**), $[Cu(TMG6Brqu)_2Br]Br \cdot 2\ CH_3CN \cdot {}^1/_2\ C_7H_8$ (**C2-II**), $[Cu(TMG6Methoxyqu)_2]Br$ (**C3-I**), $[Cu(TMG6Methoxyqu)_2Br]Br$ (**C3-II**), $[Cu(TMG6NMe_2qu)_2]Br$ (**C4-I**) and $[Cu(TMG6NMe_2qu)_2Br]Br \cdot 2\ CH_3CN$ (**C4-II**) were characterised concerning their molecular composition, bond lengths, angles, conformation of the catalysts and structural parameters ρ, τ_4 and τ_5 (Table 1 for Cu^I complexes and Table 2 for Cu^{II} complexes). The molecular structures of the Cu^I and Cu^{II} complexes are shown in Figure 1 and 2. The molecular structures of the CuBr complexes can be separated into two classes. The ligands TMG6Methoxyqu and

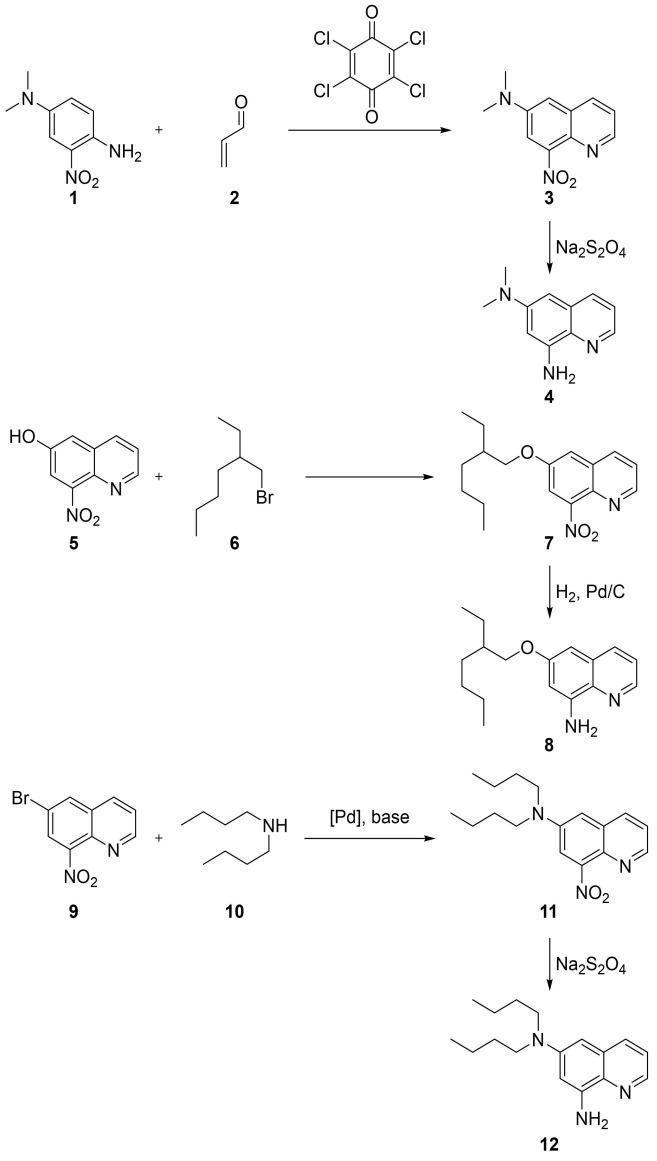

Scheme 3. Synthetic routes to amines for guanidine ligand synthesis.

TMG6NMe$_2$qu form homoleptic bischelate cationic complexes with non-coordinating bromide counterions like the unsubstituted TMGqu complex. The ligands TMG6Brqu and TMG6NO$_2$qu form neutral monochelate complexes with coordinating bromide ligands.

The average values of the Cu-N$_{GUA}$ bond lengths of the bischelate complexes are elongated compared to the monochelate complexes. However, this is not observable for the Cu-N$_{qu}$ bond lengths. For the bischelate complexes, no trend for the Cu-N$_{GUA}$ bond lengths can be observed for the different substitution patterns. The values are very similar. In contrast, the average Cu-N$_{qu}$ bond length for the bischelate complexes becomes sligthly longer with stronger electron donating properties of the substituent (Cu–N$_{qu}$ TMGqu: 1.981 Å, TMG6Methoxyqu: 1.990 Å, TMG6NMe$_2$qu: 2.021 Å). These three complexes exhibit a strongly distorted tetrahedral coordination with relative constant values of $\tau_4 \approx 0.6$. The constant values of $\rho \approx 0.98$ indicate delocalized guanidine functions. This is also the case for the monochelate complexes with values of $\rho \approx 1$. There are no trends observable related to the substitution at the 6- position of the quinoline.

The CuBr$_2$ complexes with these ligands crystallized in distorted trigonal-bipyramidal configurations with two coordinating guanidine ligands and one bromide ligand. The average Cu–N bonds lengths are shorter compared to those of the Cu^{I}-complexes. Furthermore, no trends for bond lengths and structure parameters related to the substituents are recognizable. The average Cu-N$_{GUA}$ bond lengths have a range from 2.05 Å to 2.09 Å and the Cu–N$_{qu}$ bond lengths are equal within the 3σ confidence interval independent of the substitution of the quinoline moiety. In all complexes the N$_{qu}$(1)–Cu–N$_{qu}$(2) angle is the largest at the copper center. For the unsubstituted TMGqu complex and for **C1-II**, **C2-II** and **C4-II** the second largest angle is the one between the guanidine N-donors and the copper centre. In this comparison, **C3-II** is the only complex where the N$_{GUA}$(1)-Cu–Br angle is the second largest.

The values of the τ_5 parameter and thus the coordination around the copper center are close together with τ_5 values in the range 0.73–0.79. Only the structure of **C1-II** differs with $\tau_5 =$ 0.92 indicating only a very small amount of distortion. The ρ values are constant around 1 and consequently the electrons of the guanidine function are well delocalized.

Electrochemistry

Previous studies have shown that the redox potential of a Cu^{I}/Cu^{II} couple can indicate its performance during ATRP reactions.[9–10,22] Therefore, cyclic voltammetry studies have been carried out for further investigations. The experiments were performed in acetonitrile at room temperature and two equivalents of the examined ligands were stirred with CuBr$_2$ before each experiment to ensure the *in-situ* formation of the bischelate deactivator complex. The formation of bischelate complexes of various TMGqu ligands including TMG6Methoxyqu with copper salts in solution has been described by our group in previous electrochemical studies.[16] All measurements were carried out threefold with four different sweep rates to determine the reversibility of the electrochemical reactions. As seen in Figure 3, the half potential $E_{1/2}$ was determined with respect to a Fc/Fc$^+$ internal standard and later recalculated to the SCE reference for simplified literature comparison.[23]

For all copper bromido complexes with the ligands **L1**–**L6** cyclic voltammetry measurements were conducted. Values of the half potentials $E_{1/2}$ can be found in Table S3 in the Supporting Information. For illustration, the values of $E_{1/2}$ can also be found in Figure 4.

Upon implementation of electron donating substituents such as alkoxy or alkylamine groups the redox potentials of the corresponding CuBr$_2$ complexes are shifted to the more reductive range. The incorporation of a strong electron accepting substituent such as a nitro group at the ligand C6 position

Table 1. Key bond lengths, angles and geometrical factors of the CuBr complexes [CuLBr] (L = TMG6NO$_2$qu, TMG6Brqu) and [Cu(L)$_2$]Br (L = TMGqu, TMG6Methoxyqu, TMG6NMe$_2$qu).

			Bond lengths [Å]		
Complex number Ligand	- TMGqu[11a]	C1-I TMG6NO$_2$qu	C2-I TMG6Brqu	C3-I TMG6Methoxyqu	C4-I TMG6NMe$_2$qu
Cu–N$_{GUA}$ (1)	2.118(2)	2.076(2)	2.067(3)	2.131(3)	2.141(2)
Cu–N$_{GUA}$ (2)	2.125(2)	–	–	2.116(3)	2.1036(19)
Cu–N$_{qu}$ (1)	1.987(2)	2.005(2)	2.029(3)	1.979(4)	1.999(2)
Cu–N$_{qu}$ (2)	1.974(2)	–	–	2.000(4)	2.043(2)
Cu–Br	–	2.2493(4)	2.2733(6)	–	–
			Bond angles [°]		
N$_{GUA}$ (1)–Cu-N$_{GUA}$ (2)	127.0(1)	–	–	131.21(14)	132.74(8)
N$_{qu}$ (1)–Cu–N$_{qu}$ (2)	150.9(1)	–	–	141.50(14)	143.52(8)
N$_{GUA}$ (1)–Cu–Br	–	129.77(6)	133.29 (8)	–	–
N$_{qu}$ (1)–Cu–Br	–	147.96 (6)	143.37 (9)	–	–
			Geometrical factors		
τ_4[a]	0.58	–	–	0.62	0.59
ρ[b]	0.98	0.99	1.00	0.97	0.98

[a] $\tau_4 = \frac{360°-(\alpha+\beta)}{141}$. A τ_4 value of 1 is found in ideal tetrahedral complexes where a τ_4 value of 0 is found in ideal square planar complexes.[17c] [b] $\rho = \frac{2a}{(b+c)}$ with a = d(C$_{GUA}$- N$_{GUA}$) and b and c = d(C$_{GUA}$-N$_{amine}$).[17e] Average ρ-values of two guanidine moieties.

Table 2. Key bond lengths, angles and geometrical factors of the CuBr$_2$ complexes [Cu(L)$_2$Br]Br (L = TMGqu, TMG6NO$_2$qu, TMG6Brqu, TMG6Methoxyqu, TMG6NMe$_2$qu).

			Bond lengths [Å]		
Complex number Ligand	– TMGqu[11a]	C1-II TMG6NO$_2$qu	C2-II TMG6Brqu	C3-II TMG6Methoxyqu	C4-II TMG6NMe$_2$qu
Cu–N$_{GUA}$ (1)	2.051(7)	2.064(4)	2.048(3)	2.055(4)	2.036(7)
Cu–N$_{GUA}$ (2)	2.052(7)	2.072(4)	2.077(3)	2.122(4)	2.069(7)
Cu–N$_{qu}$ (1)	1.971(7)	1.971(4)	1.976(3)	1.983(4)	1.979(6)
Cu–N$_{qu}$ (2)	1.979(7)	1.973(4)	1.980(3)	1.966(4)	1.969(6)
Cu–Br	2.663(2)	2.5180(8)	2.5745(6)	2.5461(7)	2.5963(12)
			Bond angles [°]		
N$_{GUA}$ (1)–Cu–N$_{GUA}$ (2)	131.4(3)	123.27(16)	128.11(11)	121.18(14)	130.1(3)
N$_{qu}$ (1)–Cu–N$_{qu}$ (2)	174.8(3)	178.33(17)	175.24(12)	176.99(16)	174.5(3)
N$_{GUA}$ (1)–Cu–Br	127.4(2)	122.86(12)	121.04(8)	133.38(11)	121.7(2)
			Geometrical factors		
τ_5[a]	0.72	0.92	0.79	0.73	0.74
ρ[b]	1.01	1.01	1.01	1.00	1.00

[a] $\tau_5 = \frac{(\alpha-\beta)}{60}$. A τ_5 value of 1 is found in ideal trigonal bipyramidal complexes were a τ_5 value of 0 is found in ideal square-based pyramidal complexes.[17d] [b] $\rho = \frac{2a}{(b+c)}$ with a = d(C$_{GUA}$- N$_{GUA}$) and b and c = d(C$_{GUA}$-N$_{amine}$).[17e] Average ρ-values of two guanidine moieties.

leads to a positive shift of the redox potential. The introduction of a bromide substituent leads to a slight decrease of the complexes' half potential which indicates that the positive mesomeric effect of the unpaired electrons overcomes the negative inductive effect due to the high electronegativity of the bromine atom.

As expected, CuBr$_2$ complexes with alkyl amine substituted ligands such as TMG6dBAqu and TMG6NMe$_2$qu exhibit stronger negative potential shifts than complexes derived from the TMG6Methoxyqu and TMG6EHOqu ligands. Based on these data, the ATRP equilibrium constants of the amino substituted complexes should be larger than those of the alkoxy ligands. Likewise, the polymerization rate should be increased.

Atom Transfer Radical Polymerization

Determination of K_{ATRP}

In addition to the position of the ATRP equilibrium K_{ATRP} influences the polymerization rate and control. High values

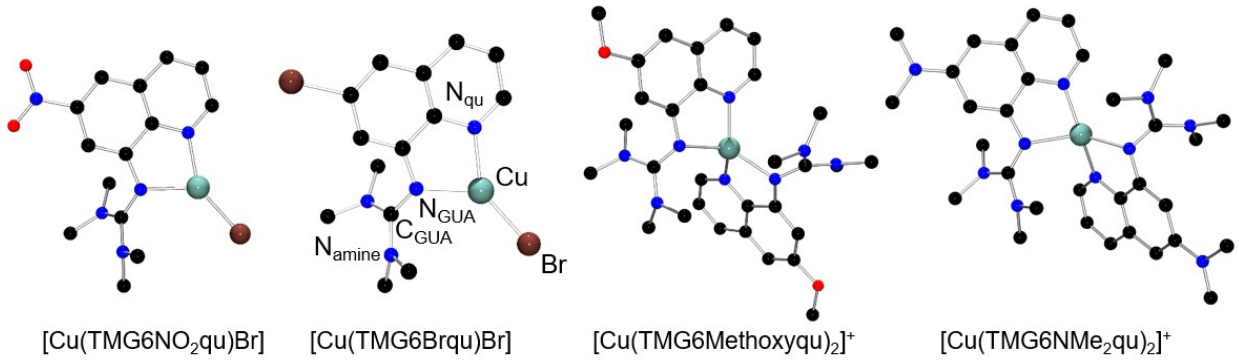

Figure 1. Molecular structures of the complexes in crystals of **C1-I** - **C2-I** in the solid state or of the cationic complex units in crystals of **C3-I** - **C4-I** in the solid state. Key atoms are exemplarily marked in one complex. H atoms and anions are omitted for clarity.

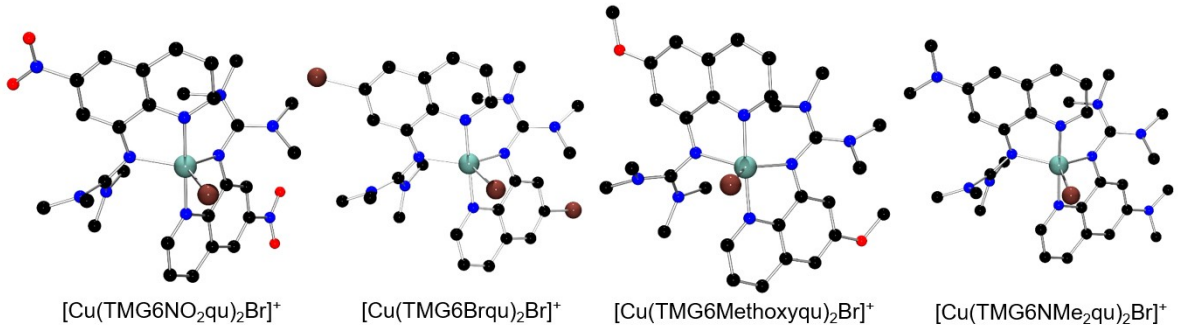

Figure 2. Molecular structures of the cationic complex units in crystals of **C1-II** - **C4-II** in the solid state. H atoms, solvents and anions are omitted for clarity.

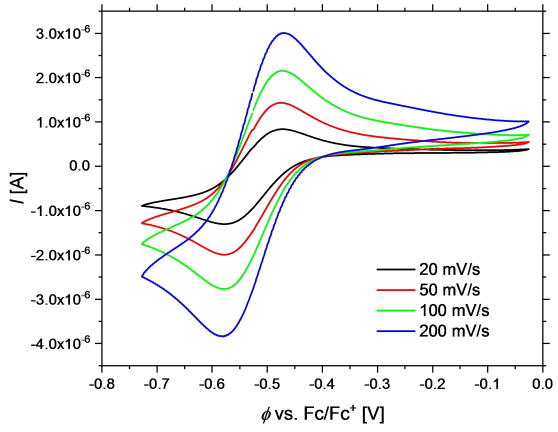

Figure 3. Cyclic voltammograms of the $[Cu^{I}(TMG6Methoxyqu)_2]^+$/$[Cu^{II}(TMG6Methoxyqu)_2Br]^+$ couple at different sweep rates starting from $[Cu^{II}(TMG6Methoxyqu)_2Br]Br$ in MeCN at 25 °C.

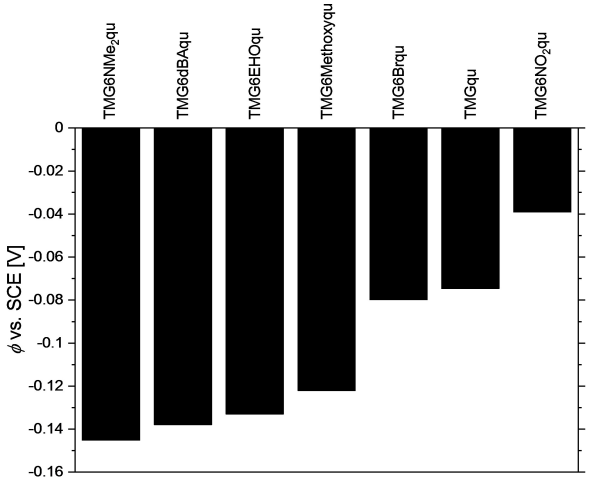

Figure 4. Redox potentials of various $[Cu^{I}L_2]^+/[Cu^{II}L_2Br]^+$ couples with L = TMGqu[11a], $TMG6NO_2qu$, TMG6Brqu, TMG6Methoxyqu, TMG6EHOqu, TMG6dBAqu and $TMG6NMe_2qu$.

promise the possibility of low catalyst concentrations and activity for less reactive monomers.

For the determination of K_{ATRP} by UV/Vis spectroscopy the measurement starts with the Cu^{I} complex which reacts with the initiator ethyl α-bromoisobutyrate (EBrib) to the Cu^{II} complex. The evolution of the Cu^{II} species can be followed due to the characteristic d-d transition band at around 900–950 nm. Two methods for K_{ATRP} determination have been developed by

Fischer and Fukuda[24] and by Matyjaszewski et al.[4a] Both rely on the monitoring of the Cu^{II} absorption band. The resulting plots for both methods can be found in the Supporting Information (Figures S5–S9). K_{ATRP} constants were measured for copper catalyst systems based on **L2**–**L6** under the same conditions like previously reported measurements of guanidine quinoline complexes.[10] Resulting values are summarized in Table 3.

As expected for more reducing catalyst systems higher values for K_{ATRP} can be achieved. The lowest value belongs to the Br substituted system, and analogously to the order of electrochemical potentials the values of K_{ATRP} increase up to the NMe_2 substituted system. In general lower values are determined by the method according to Fischer and Fukuda.

The achieved results for K_{ATRP} and $E_{1/2}$ are plotted into the correlation published from Matyjaszewski *et al.*[25] and help to classify the activity of catalyst systems (Figure 5). The systems presented here fit well to the linear regression. The measurements were reproduced four times with different complex and initiator solutions to minimize errors. The values of the systems with electron pushing moieties promise a high activity in polymerization reactions due to the lager equilibrium constants and the more negative potentials. Compared to other bidentate systems like substituted bipyridine based catalysts the here presented complexes show promising properties. Only the ligand $(Me)_2$–N–bpy (left of Scheme 1) system has lower (more reducing) values for the potential.[8]

Table 3. K_{ATRP} for $[Cu(L)_2]^+/[Cu(L)_2Br]^+$ equilibrium. L = TMGqu, TMG6NMe_2qu, TMG6dBAqu, TMG6Methoxyqu, TMG6EHOqu, TMG6Brqu.

$[Cu(L)_2]^+/[Cu(L)_2Br]^+$, L =	K_{ATRP} (Matyjaszewski)	K_{ATRP} (Fischer-Fukuda)
TMGqu[10]	$8.6 \pm 0.5 \times 10^{-8}$	–
TMG6NMe_2qu	$3.58 \pm 0.11 \times 10^{-7}$	$2.55 \pm 0.04 \times 10^{-7}$
TMG6dBAqu	$3.16 \pm 0.13 \times 10^{-7}$	$2.31 \pm 0.06 \times 10^{-7}$
TMG6Methoxyqu	$1.54 \pm 0.19 \times 10^{-7}$	$1.26 \pm 0.03 \times 10^{-7}$
TMG6EHOqu	$1.52 \pm 0.10 \times 10^{-7}$	$1.24 \pm 0.06 \times 10^{-7}$
TMG6Brqu	$3.61 \pm 0.39 \times 10^{-8}$	$3.40 \pm 0.17 \times 10^{-8}$

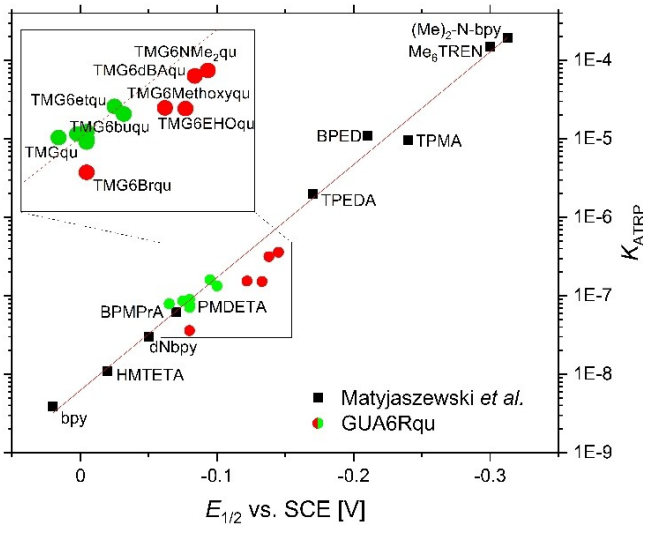

Figure 5. Correlation of $E_{1/2}$ and K_{ATRP} (measured with EBrib at 22 °C in MeCN) for different copper complexes coordinated by multidentate N-donor ligands. Black squares: Values published by Matyjaszewski *et al.*[25] Green circles: GUA6Rqu values published by Herres-Pawlis *et al.*[10] Red circles: New values for GUA6Rqu complexes.

Determination of k_{act} and k_{deact}

Next to K_{ATRP} the rate constants k_{act} and k_{deact} for activation and deactivation, respectively, are very important for ATRP catalysts because a fast exchange between the active and dormant chains is essential for narrow molar mass distributions. This is especially necessary for polymerization methods with low catalyst concentrations.[26]

The direct measurement of k_{deact} is rather complicated[27] which is why k_{act} measurements via time-dependent UV/Vis spectroscopy are used to calculate k_{deact} afterwards with known K_{ATRP} values. The measurement of k_{act} follows a protocol published by Matyjaszewski *et al.* whilst the Cu^{I} complex reacts with a tenfold excess of initiator (EBrib) and radical trapping agent (2,2,6,6-tetramethylpiperidinyl-1-oxyl, TEMPO) to the Cu^{II} complex.[28] These conditions enable a pseudo-first-order reaction and no deactivation reaction can occur. The final absorbances were further used to determine values of the extinction coefficients ε. Analogous to the K_{ATRP} measurements the increase of the deactivator complex was followed on the same d-d transition band by UV/Vis spectroscopy. The course of the absorbance can be fitted using the equation $A = A_0\left(1 - e^{-k_{obs}t}\right) + C$ and later on k_{act} can be obtained through the equation $k_{act} = k_{obs}/[I]_0$. The raw data with the fits can be found in the Supporting Information (Figure S10 to S14) and the calculated values for k_{act} and k_{deact} are shown in Table 4. As expected the activation reaction of systems with electron donating groups is faster in line with the more negative the redox potentials. The slowest activation reaction proceeds with the bromine substituted ligand **L2**. Faster are the OMe substituted ligand **L3** and the alkylated derivative **L5** with almost similar values. The amine substituted ligands exhibit the fastest activation reactions whereas the ligand with methyl groups **L4** is even faster than **L6** with butyl chains. For the

Table 4. k_{act} and k_{deact} for $[Cu(L)_2]^+/[Cu(L)_2Br]^+$ equilibrium. L = TMGqu, TMG6NMe_2qu, TMG6dBAqu, TMG6Methoxyqu, TMG6EHOqu, TMG6Brqu.

$[Cu(L)_2]^+/[Cu(L)_2Br]^+$, L =	k_{act} [L mol^{-1} s^{-1}]	k_{deact} ($= k_{act}/K_{ATRP}$) [L mol^{-1} s^{-1}]
TMGqu[10]	0.83 ± 0.03	$9.7 \pm 0.3 \times 10^6$
TMG6NMe_2qu (**L4**)	2.33 ± 0.04	$6.46 \pm 0.31 \times 10^6$
TMG6dBAqu (**L6**)	1.88 ± 0.03	$5.88 \pm 0.31 \times 10^6$
TMG6Methoxyqu (**L3**)	1.12 ± 0.04	$7.43 \pm 1.24 \times 10^6$
TMG6EHOqu (**L5**)	1.25 ± 0.03	$8.36 \pm 0.80 \times 10^6$
TMG6Brqu (**L2**)	0.345 ± 0.004	$9.57 \pm 1.14 \times 10^6$

determination of k_{deact} the K_{ATRP} values obtained by the Matyjaszewski method were used. As expected the resulting rate constants for the deactivation reaction slightly decrease for more electron-rich catalysts but all complexes show sufficiently high values to perform standard ATRP.[22]

Polymerization kinetics

All polymerization reactions of styrene were conducted in benzonitrile as solvent. This enables a better comparability of the performance between the good solubility and poor solubility systems in pure styrene. Benzonitrile was chosen because it combines the miscibility with styrene and the solubility of the here used complexes. EBrib as initiator was used and ratios of monomer (M)/initiator (I)/catalyst (C) = 100/1/1 were targeted. It was expected that the activity in ATRP increases by the order of equilibrium constants and potentials from the catalysts. Following this order no polymer with the system based on TMG6NO$_2$qu (**L1**) was observed within two days. All other systems were able to polymerize styrene under controlled conditions yielding a constant slope of conversion, molar masses M_n close to the theoretical molar masses $M_{n,theo}$ and dispersities $Đ$ below 1.15. An exemplary plot of semi-logarithmic conversion against time with the assumed most active catalyst system here (based on the ligand TMG6NMe$_2$qu, **L4**) is shown in Figure 6.

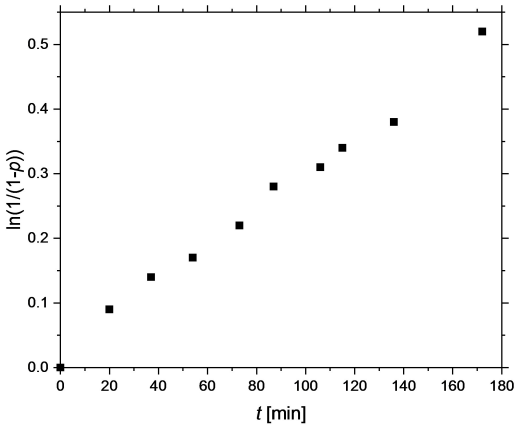

Figure 6. Semilogarithmic plot of conversion vs. time for ATRP of styrene in benzonitrile catalysed by [Cu(TMG6NMe$_2$qu)$_2$]Br and EBrib as initiator. Conditions:110 °C; Ratio: M/I/C = 100/1/0.5.

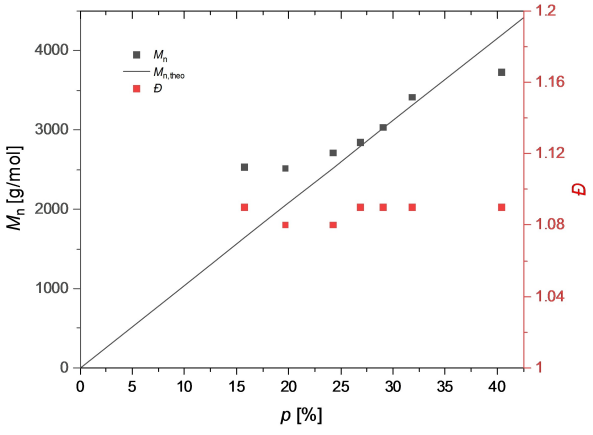

Figure 7. M_n, $M_{n,theo}$ and $Đ$ vs. conversion for ATRP of styrene in benzonitrile catalysed by [Cu(TMG6NMe$_2$qu)$_2$]Br and EBrib as initiator. Conditions:110 °C; Ratio: M/I/C = 100/1/0.5.

The catalyst concentration of this polymerization and also for the one with the catalyst based on the ligand TMG6dBAqu (**L6**) were lowered to ratios of 100/1/0.5 and 100/1/0.6. This is due to the fact that under the intended conditions the kinetic parameters deviated strongly from ideal behavior assuming that termination reactions occur. Nevertheless with this catalyst concentrations linear slopes can be achieved indicating controlled conditions which are supported by good accordance of M_n compared to $M_{n,theo}$ and low $Đ$ values (Figure 7). This logarithmic course against conversion is also representative for all other polymerization experiments conducted with the catalysts presented in here. The increased M_n values compared to $M_{n,theo}$ at lower conversions is thus justified by the workup procedure of the polymer samples. By precipitation and decantation with ethanol a loss of short chains might be possible. However, with higher conversions the molar masses are in accordance with the theoretical molar masses and the dispersities stay constant. To compare the speed of polymerizations with the catalyst systems based on the ligands **L2**–**L6**, the polymerization rate constants k_p can be considered (Table 5). The values in general follow the same order as the potentials and therefore all systems tested here show higher rate constants compared to unsubstituted TMGqu system. Excluded from this order are only the polymerizations performed with the TMG6Methoxyqu (**L3**) based catalyst. This rate constant is two and a half times higher than the constant of the system based on TMG6NMe$_2$qu (**L4**).

A reason might be that the used conditions are ideal for this specific system by a small radical concentration to suppress termination reactions but simultaneously large enough to foster a high polymerization rate. For polymerizations mediated by catalysts based on TMG6NMe$_2$qu (**L4**) and TMG6dBAqu (**L6**) the lower k_p values could be explained by the potentials and the PRE. A lower potential effects that more Cu^{II} complex and radicals at the beginning of the reaction are formed. As consequence more termination reactions occur, the deactivator species accumulates and the equilibrium shifts to the dormant

Table 5. ATRP of styrene in benzonitrile (if not stated otherwise) initiated by EBrib and catalysed by Cu/L$_2$ catalyst systems.

L =	M/I/C	k_p [L mol^{-1} s^{-1}]
TMGqu[11a]	100/1/1	6.3×10^{-4}
TMG6NMe$_2$qu	100/1/0.5	$1.3\times10^{-3}\pm1.9\times10^{-4}$
TMG6dBAqu	100/1/0.6	$1.1\times10^{-3}\pm1.8\times10^{-4}$
TMG6Methoxyqu	100/1/1	$3.4\times10^{-3}\pm5.3\times10^{-4}$
TMG6EHOqu (bulk)	100/1/1	$7.5\times10^{-4}\pm9.9\times10^{-5}$
TMG6EHOqu	100/1/1	$7.2\times10^{-4}\pm1.4\times10^{-4}$
TMG6Brqu	100/1/1	$6.7\times10^{-4}\pm3.1\times10^{-5}$

side resulting in less active radical chains that can polymerise. This argument is confirmed with the uncontrolled conditions with higher catalyst loadings of these systems. Further a polymerization in pure styrene was conducted with the catalyst based on TMG6EHOqu (**L5**). The catalyst shows a good solubility and controlled polymerizations can be performed.

Conclusion

Six copper guanidine quinoline systems with various substituents at the 6-position of the quinoline were examined for ATRP comprising investigation of the molecular structures, electrochemistry, determination of important ATRP constants and polymerization of styrene. The syntheses of four new ligands TMG6NO_2qu, TMG6NMe_2qu, TMG6EHOqu and TMG6dBAqu have been presented. Studies with the ligands TMG6NO_2qu, TMG6Brqu, TMG6Methoxyqu and TMG6NMe_2qu gave indication how the properties can be influenced by electronic effects of substituents. The ligands TMG6EHOqu and TMG6dBAqu were synthesized to increase the solubility in apolar monomers.

Crystal structures of copper bromide complexes showed the influence on bond lengths, angles and structural parameters by the different substitutions. For Cu^{I} complexes electron rich ligand systems form bischelate complexes whereas electron poor ligands form monochelate complexes in the solid state. Further the Cu-N_{qu} bond length increases with a stronger electron donating ability of the substituent. All Cu^{II} complexes crystallized in distorted trigonal-bipyramidal configuration with two coordinating guanidine ligands and one bromide ligand. Here no trends regarding to the substitutions can be observed.

Cyclic voltammetry reveals that – as expected – more negative potentials of the copper complexes can be achieved by stronger electron pushing substituents of the ligands. The most reducing potential was achieved by NMe_2 substitution and the less reducing with the electron withdrawing NO_2 group.

Analogue to this order K_{ATRP} and k_{act} values were determined. Here the method according to Fischer and Fukuda and the method of Matyjaszewski were used. The calculated values of k_{deact} slightly decrease for more electron rich catalysts. Nevertheless concerning these results the catalyst based on the ligand TMG6NMe_2qu is the most promising.

Polymerization reactions of styrene with the catalysts based on the ligands **L2**–**L6** were conducted in solution showing controlled conditions and a high catalyst activity. The catalysis with electron rich ligands afforded faster polymerizations according the order of measured potentials. Only the catalyst based on the ligand TMG6Methoxyqu does not follow this order showing larger rate constants k_p. Introducing longer alkyl groups solubility could be improved and polymerizations in bulk with the catalyst based on **L5** are possible.

On balance the here presented results show that electronic influencing substituents at the quinoline backbone can lead to highly active bidentate ATRP catalysts. Catalysts based on amine substituted ligands **L4** and **L6** seems to be at the limit for ATRP under standard conditions due to a high radical concentration at the beginning of the polymerization. In a future perspective, these systems and similar catalysts with even lower potentials could perform ATRP with reduced concentrations and the use of regenerating techniques like ARGET ATRP might be possible. Due to solubility problems of the presented systems in pure styrene it was shown that the polarity of the complexes can be changed by alkylation and so a better solubility for a range of monomers could be conducted.

Experimental Section

General

Ligands and complexes were synthesized under nitrogen atmosphere by using Schlenk technique and a glove box for inert conditions. Dry and degassed solvents were prepared according to literature.[29] Chemicals for the synthesis of the ligands as well as Cu^{II}-salts for complex syntheses were all purchased from Grüssing, AppliChem, Acros Organics or TCI and were used as received without further purification. $Cu^{I}Cl$, $Cu^{I}Br$ and the Vilsmeier salt *N*,*N*′-*N*,*N*,*N*′,*N*′-tetramethylchloroformamidinium chloride (TMG-VS) were synthesized as described in the literature.[17a,b,30] The ligands TMG6Brqu and TMG6Methoxyqu were synthesized according to the literature.[16]

General analytical methods

FT IR: KBr FT IR spectra were measured with a ThermoFisher Avatar 360 (Resolution 2 cm^{-1}). ATR FT IR spectra where measured with a Shimadzu IRTracer 100 with CsI beamsplitter combined with a Specac Quest ATR unit (monolithic crystalline diamond, resolution 2 cm^{-1}).

MS: EI mass spectra were measured with a ThermoFisher Scientific Finnigan MAT 95 mass spectrometer. FAB mass spectra were received with a Thermo Finnigan MAT 95 or a Jeol MStation 700. Ionisation took place in 2-nitrobenzyl alcohol or glycerol as matrix on a copper target with 8 kV xenon atoms. ESI mass spectra were received with a ThermoFisher Scientific LTQ Orbitrap XL. The source voltage was 4.49 kV, the capillary temperature amounted to 299.54 °C. The tube lens voltage lay between 110 and 130 V.

^{1}H- and ^{13}C-NMR: ^{1}H- and ^{13}C-NMR spectra were measured on a Bruker Avance III HD 400 or a Bruker Avance II 400 nuclear resonance spectrometer. Measurements were conducted in fully deuterated solvents. The residual signal of the solvent served as an internal standard.

Gel permeation chromatography

The average molecular masses and the mass distributions of the yielded polystyrene samples were measured by gel permeation chromatography (GPC) in THF as mobile phase at a flow rate of 1 mL/min. The utilised GPCmax VE-2001 from Viscotek is a combination of two Malvern Viscotek T columns (porous styrene divinylbenzene copolymer) with a maximum pore size of 500 and 5000 Å, an HPLC pump and a refractive index detector (VE-3580) and a viscometer (Viscotek 270 Dual Detector). Universal calibration was applied to evaluate the chromatographic results.

UV/Vis spectroscopic setup for K_{ATRP}/k_{act} determination

UV/Vis spectroscopic measurements were conducted with an Avantes AvaSpec-ULS2048 CCD-Spectrometer and an Avantes Ava-Light-DH–S-BAL lightsource. The measurements were performed in Hellma QS-Screwcap-Cuvettes with an optical pathlength of 10.00 mm.

CV measurements

The measurements were conducted at room temperature under inert conditions with a Metrohm Autolab Potentiostat PGSTAT 101 using a three electrode arrangement with a Pt wire as counter electrode, a Pt disc working electrode (1 mm diameter) and a Ag wire as reference electrode (pseudo reference). The measurements were done in CH_3CN/0.1 mol L^{-1} NBu_4PF_6 with a sample concentration of 10 mM. Ferrocene was added afterwards as an internal standard of the sample and all potentials are referenced relative to the Fc/Fc^+ couple. Cyclic voltammograms were measured with 200 mV/s, 100 mV/s, 50 mV/s and 20 mV/s.

X-ray diffraction analysis

The single crystal diffraction data for **C1-I**, **C1-II**, **C2-I**, **C2-II**, **C3-I**, **C3-II**, **C4-I**, **C4-II** are presented in Tables S1 and S2. The data for **C4-I** were collected with an Oxford KM4 XCalibur2 and for **C1-I**, **C1-II**, **C2-I**, **C2-II**, **C3-I**, **C3-II**, **C4-II** on a Bruker D8 Venture with APEX CCD detector with graphite monochromated Mo–Kα radiation ($\lambda =$ 0.71073 Å) at 100 K in a mix of ω- and φ-scans. Data reduction and absorption correction was performed with the programs CRYSALIS (Oxford, 2008) and CRYSALIS RED (Oxford, 2008) (**C4-I**) or with SAINT and SADABS[31] (**C1-I**, **C1-II**, **C2-I**, **C2-II**, **C3-I**, **C3-II**, **C4-II**) The structure was solved by direct and conventional Fourier methods and all non-hydrogen atoms were refined anisotropically with full-matrix least-squares based on F^2 (XPREP,[32] SHELXS[33] and ShelXle[34]). Hydrogen atoms were derived from difference Fourier maps and placed at idealised positions, riding on their parent C atoms, with isotropic displacement parameters $U_{iso}(H) = 1.2U_{eq}(C)$ and $1.5U_{eq}$(C methyl). All methyl groups were allowed to rotate but not to tip.

Full crystallographic data (excluding structure factors) have been deposited with the Cambridge Crystallographic Data Centre as supplementary no. CCDC–2049173 for **C1-I**, CCDC–2049174 for **C1-II**, CCDC–2049175 for **C2-I**, CCDC–2049176 for **C2-II**, CCDC–2049177 for **C3-I**, CCDC–2049178 for **C3-II**, CCDC–2049179 for **C4-I** and CCDC–2049180 **C4-II**. Copies of the data can be obtained free of charge on application to CCDC, 12 Union Road, Cambridge CB2 1EZ, UK (fax: (+44)1223-336-033; e-mail: deposit@ccdc.cam.ac.uk).

Polymerization procedure

Styrene (Acros Organics, 99% stab.) and the initiator ethyl α-bromoisobutyrate (EBrib, abcr, 98%) have been purified by distillation over CaH_2. All polymerizations were conducted with *in situ* generated catalysts. First CuBr (0.23 mmol, 1 eq.), then ligand (0.46 mmol, 2 eq.) were directly weighed into the polymerization vessel under nitrogen atmosphere inside a glovebox. Outside the glove box styrene (23 mmol, 100 eq.), benzonitrile (1.13 mL) and finally the initiator EBrib (0.23 mmol, 1 eq.) were added with gastight glass syringes using Schlenk technique.

After addition of the initiator, the solution was heated to 110 °C under vigorous stirring. The first aliquot was taken with a glass pipette under inert conditions after 2.5 min. At this point of time the polymerization mixture reached its desired temperature and thus was chosen to be starting point of the polymerization. Further samples were taken in certain time intervals. The samples were diluted in $CDCl_3$ followed by a ^{1}H-NMR spectroscopy measurement to determine the conversion. Afterwards the polymer was precipitated in ethanol to remove the copper complex and residual monomer. The solid, colourless polystyrene was dried overnight at 50 °C and molecular mass distributions were measured by GPC.

K_{ATRP} determination

All measurements were conducted in oxygen free acetonitrile at 22 °C. The acetonitrile has been degassed by three *freeze-pump-thaw* cycles. Stock solutions of the complexes and the cuvettes were prepared in a glovebox under inert conditions.

During the measurement in the cuvette (2 mL) the concentration of complex and initiator was 5 mM.

First, stock solutions of the initiator (1.00 mmol EBrib in 10 mL of acetonitrile) and the complexes (0.05 mmol $Cu^{I}Br$ and 0.1 mmol ligand in 2 mL of acetonitrile) were prepared. A screw cap cuvette containing a stirring bar was filled with 1.5 mL of acetonitrile and tightly sealed with a silicon septum. After addition of 400 µL catalyst solution the UV/Vis spectroscopic measurement was started. 100 µL of EBrib solution were added and the formation of the Cu^{II} species was followed via UV/Vis spectroscopy.

k_{act} determination

All measurements were performed in oxygen free acetonitrile at 22 °C. The acetonitrile has been degassed by three *freeze-pump-thaw* cycles. Stock solutions of the complexes and the cuvettes were prepared in a glovebox under inert conditions.

During the measurement in the cuvette (2 mL) the concentration of the complex was 3 mM. A tenfold excess of initiator and trapping agent (30 mM) was used.

First, stock solutions of the initiator (6.00 mmol EBrib in 10 mL of solvent), the trapping agent (6.00 mmol TEMPO in 10 mL solvent) and the complexes (0.05 mmol CuBr and 0.1 mmol ligand in 2 mL of solvent) were prepared.

A screw cap cuvette containing a stirring bar was filled with 1.26 mL acetonitrile and tightly sealed with a silicon septum. After addition of 100 µL initiator and 400 µL TEMPO solution the UV/Vis spectroscopic measurement was started. By adding 240 µL of complex solution the reaction was initiated and the formation of the Cu^{II} species was followed via UV/Vis spectroscopy.

Acknowledgements

J.S.M. thanks the Konrad-Adenauer-Stiftung for generous financial support in form of a fellowship. Open access funding enabled and organized by Projekt DEAL.

Keywords: Copper · Atom transfer radical polymerization · Kinetics · Guanidines · Ligand design

[1] a) J.-S. Wang, K. Matyjaszewski, *Macromolecules* **1995**, *28*, 7901–7910; b) V. Percec, B. Barboiu, *Macromolecules* **1995**, *28*, 7970–7972; c) M. Kato, M. Kamigaito, M. Sawamoto, T. Higashimura, *Macromolecules* **1995**, *28*, 1721–1723.

[2] a) K. Min, H. Gao, K. Matyjaszewski, *J. Am. Chem. Soc.* **2005**, *127*, 3825–3830; b) W. Jakubowski, K. Matyjaszewski, *Angew. Chem. Int. Ed.* **2006**, *45*, 4482–4486; *Angew. Chem.* **2006**, *118*, 4594–4598; c) A. J. D. Magenau, N. C. Strandwitz, A. Gennaro, K. Matyjaszewski, *Science* **2011**, *332*, 81–84; d) N. Bortolamei, A. A. Isse, A. J. D. Magenau, A. Gennaro, K. Matyjaszewski, *Angew. Chem. Int. Ed.* **2011**, *50*, 11391–11394; *Angew. Chem.* **2011**, *123*, 11593–11596; e) A. E. Enciso, L. Fu, A. J. Russell, K. Matyjaszewski, *Angew. Chem. Int. Ed.* **2018**, *57*, 933–936; *Angew. Chem.* **2018**, *130*, 945–948; f) Z. Wang, J. Yan, T. Liu, Q. Wei, S. Li, M. Olszewski, J. Wu, J. Sobieski, M. Fantin, M. R. Bockstaller, K. Matyjaszewski, *ACS Macro Lett.* **2019**, *8*, 859–864; g) X. Lin, G. Xie, S. Liu, M. R. Martinez, Z. Wang, H. Lou, R. Fu, D. Wu, K. Matyjaszewski, *ACS Appl. Mater. Interfaces* **2019**, *11*, 18763–18769.

[3] C. Y. Lin, M. L. Coote, A. Gennaro, K. Matyjaszewski, *J. Am. Chem. Soc.* **2008**, *130*, 12762–12774.

[4] a) W. Tang, N. V. Tsarevsky, K. Matyjaszewski, *J. Am. Chem. Soc.* **2006**, *128*, 1598–1604; b) H. Fischer, *J. Polym. Sci. Part A* **1999**, *37*, 1885–1901.

[5] P. Krys, K. Matyjaszewski, *Eur. Polym. J.* **2017**, *89*, 482–523.

[6] a) M. C. Iovu, K. Matyjaszewski, *Macromolecules* **2003**, *36*, 9346–9354; b) K. Matyjaszewski, W. Jakubowski, K. Min, W. Tang, J. Huang, W. A. Braunecker, N. V. Tsarevsky, *Proc. Natl. Acad. Sci. USA* **2006**, *103*, 15309–15314.

[7] W. Tang, K. Matyjaszewski, *Macromolecules* **2006**, *39*, 4953–4959.

[8] A. J. D. Magenau, Y. Kwak, K. Schröder, K. Matyjaszewski, *ACS Macro Lett.* **2012**, *1*, 508–512.

[9] T. G. Ribelli, M. Fantin, J.-C. Daran, K. F. Augustine, R. Poli, K. Matyjaszewski, *J. Am. Chem. Soc.* **2018**, *140*, 1525–1534.

[10] T. Rösener, A. Hoffmann, S. Herres-Pawlis, *Eur. J. Inorg. Chem.* **2018**, *2018*, 3164–3175.

[11] a) T. Rösener, O. Bienemann, K. Sigl, N. Schopp, F. Schnitter, U. Flörke, A. Hoffmann, A. Döring, D. Kuckling, S. Herres-Pawlis, *Chem. Eur. J.* **2016**, *22*, 13550–13562; b) T. Rösener, K. Kröckert, A. Hoffmann, S. Herres-Pawlis, *Z. Anorg. Allg. Chem.* **2018**, *644*, 1317–1328; c) A. Hoffmann, O. Bienemann, I. D. S. Vieira, S. Herres-Pawlis, *Polymer* **2014**, *6*, 995–1007; d) A. Hoffmann, O. Bienemann, I. d. S. Vieira, S. Herres-Pawlis, *Z. Naturforsch. B* **2014**, *69*, 589; e) O. Bienemann, A.-K. Froin, I. dos Santos Vieira, R. Wortmann, A. Hoffmann, S. Herres-Pawlis, *Z. Anorg. Allg. Chem.* **2012**, *638*, 1683–1690; f) O. Bienemann, R. Haase, A. Jesser, T. Beschnitt, A. Döring, D. Kuckling, I. dos Santos Vieira, U. Flörke, S. Herres-Pawlis, *Eur. J. Inorg. Chem.* **2011**, *2011*, 2367–2379; g) O. Bienemann, R. Haase, U. Flörke, A. Döring, D. Kuckling, S. Herres-Pawlis, *Z. Naturforsch. B* **2010**, *65*, 798; h) S. H. Oakley, M. P. Coles, P. B. Hitchcock, *Inorg. Chem.* **2003**, *42*, 3154–3156; i) A. S. Brar, S. Kaur, *J. Polym. Sci. Part A* **2005**, *43*, 5906–5922; j) D. Petrovic, L. M. R. Hill, P. G. Jones, W. B. Tolman, M. Tamm, *Dalton Trans.* **2008**, 887–894.

[12] a) A. Metz, R. Plothe, B. Glowacki, A. Koszalkowski, M. Scheckenbach, A. Beringer, T. Rösener, J. Michaelis de Vasconcellos, R. Haase, U. Flörke, A. Hoffmann, S. Herres-Pawlis, *Eur. J. Inorg. Chem.* **2016**, *2016*, 4974–4987; b) P. M. Schäfer, M. Fuchs, A. Ohligschläger, R. Rittinghaus, P. McKeown, E. Akin, M. Schmidt, A. Hoffmann, M. A. Liauw, M. D. Jones, S. Herres-Pawlis, *ChemSusChem* **2017**, *10*, 3547–3556; c) P. M. Schäfer, P. McKeown, M. Fuchs, R. D. Rittinghaus, A. Hermann, J. Henkel, S. Seidel, C. Roitzheim, A. N. Ksiazkiewicz, A. Hoffmann, A. Pich, M. D. Jones, S. Herres-Pawlis, *Dalton Trans.* **2019**, *48*, 6071–6082; d) R. D. Rittinghaus, P. M. Schäfer, P. Albrecht, C. Conrads, A. Hoffmann, A. N. Ksiazkiewicz, O. Bienemann, A. Pich, S. Herres-Pawlis, *ChemSusChem* **2019**, *12*, 2161–2165.

[13] a) F. Strassl, B. Grimm-Lebsanft, D. Rukser, F. Biebl, M. Biednov, C. Brett, R. Timmermann, F. Metz, A. Hoffmann, M. Rübhausen, S. Herres-Pawlis, *Eur. J. Inorg. Chem.* **2017**, *2017*, 3350–3359; b) S. Herres-Pawlis, R. Haase, P. Verma, A. Hoffmann, P. Kang, T. D. P. Stack, *Eur. J. Inorg. Chem.* **2015**, *2015*, 5426–5436; c) M. Schatz, V. Raab, S. P. Foxon, G. Brehm, S. Schneider, M. Reiher, M. C. Holthausen, J. Sundermeyer, S. Schindler, *Angew. Chem. Int. Ed.* **2004**, *43*, 4360–4363; *Angew. Chem.* **2004**, *116*, 4460–4464; d) C. Würtele, E. Gaoutchenova, K. Harms, M. C. Holthausen, J. Sundermeyer, S. Schindler, *Angew. Chem. Int. Ed.* **2006**, *45*, 3867–3869; *Angew. Chem.* **2006**, *118*, 3951–3954; e) D. Maiti, D.-H. Lee, K. Gaoutchenova, C. Würtele, M. C. Holthausen, A. A. Narducci Sarjeant, J. Sundermeyer, S. Schindler, K. D. Karlin, *Angew. Chem. Int. Ed.* **2008**, *47*, 82–85; *Angew. Chem.* **2008**, *120*, 88–91; f) J. S. Woertink, L. Tian, D. Maiti, H. R. Lucas, R. A. Himes, K. D. Karlin, F. Neese, C. Würtele, M. C. Holthausen, E. Bill, J. Sundermeyer, S. Schindler, E. I. Solomon, *Inorg. Chem.* **2010**, *49*, 9450–9459.

[14] B. Dicke, A. Hoffmann, J. Stanek, M. S. Rampp, B. Grimm-Lebsanft, F. Biebl, D. Rukser, B. Maerz, D. Göries, M. Naumova, M. Biednov, G. Neuber, A. Wetzel, S. M. Hofmann, P. Roedig, A. Meents, J. Bielecki, J. Andreasson, K. R. Beyerlein, H. N. Chapman, C. Bressler, W. Zinth, M. Rübhausen, S. Herres-Pawlis, *Nat. Chem.* **2018**, *10*, 355–362.

[15] a) J. Stanek, N. Sackers, F. Fink, M. Paul, L. Peters, R. Grunzke, A. Hoffmann, S. Herres-Pawlis, *Chem. Eur. J.* **2017**, *23*, 15738–15745; b) A. Hoffmann, J. Stanek, B. Dicke, L. Peters, B. Grimm-Lebsanft, A. Wetzel, A. Jesser, M. Bauer, M. Gnida, W. Meyer-Klaucke, M. Rübhausen, S. Herres-Pawlis, *Eur. J. Inorg. Chem.* **2016**, *2016*, 4731–4743.

[16] J. Stanek, M. Konrad, J. Mannsperger, A. Hoffmann, S. Herres-Pawlis, *Eur. J. Inorg. Chem.* **2018**, *2018*, 4997–5006.

[17] a) W. Kantlehner, E. Haug, W. W. Mergen, P. Speh, T. Maier, J. J. Kapassakalidis, H.-J. Bräuner, H. Hagen, *Liebigs Ann. Chem.* **1984**, *1984*, 108–126; b) S. Herres-Pawlis, U. Flörke, G. Henkel, *Eur. J. Inorg. Chem.* **2005**, *2005*, 3815–3824; c) L. Yang, D. R. Powell, R. P. Houser, *Dalton Trans.* **2007**, 955–964; d) A. W. Addison, T. N. Rao, J. Reedijk, J. van Rijn, G. C. Verschoor, *J. Chem. Soc. Dalton Trans.* **1984**, 1349–1356; e) V. Raab, K. Harms, J. Sundermeyer, B. Kovačević, Z. B. Maksić, *J. Org. Chem.* **2003**, *68*, 8790–8797.

[18] J. Schofield, R. K. Smalley, D. I. C. Scopes, *Chem. Ind.* **1986**, 587.

[19] T. Maier, T. Beckers, T. Baer, M. Vennemann, V. Gekeler, A. Zimmermann, P. Gimmnich, K. J. Padiya, H. Joshi, U. Joshi, M. Makhija, *Vol. WO 2009037001A2*, Germany, **2009**.

[20] G. Wielgosz-collin, M. Duflos, P. Pinson, G. Le baut, P. Renard, C. Bennejean, J. Boutin, M. Boulanger, *J. Enzyme Inhib. Med. Chem.* **2002**, *17*, 449–453.

[21] a) D. Smil, S. Leit, A. Ajamian, M. Allan, Y. A. Chantigny, R. Deziel, E. Therrien, A. Wahhab, S. Manku, *Vol. 2007/0293530A1*, US, **2007**; b) R. E. Mewshaw, P. Zhou, D. Zhou, K. L. Maeagher, M. Asselin, D. A. Evrard, A. M. Gilbert, *Vol. 6,313,126 B1*, US, **2001**.

[22] W. Tang, Y. Kwak, W. Braunecker, N. V. Tsarevsky, M. L. Coote, K. Matyjaszewski, *J. Am. Chem. Soc.* **2008**, *130*, 10702–10713.

[23] N. G. Connelly, W. E. Geiger, *Chem. Rev.* **1996**, *96*, 877–910.

[24] a) H. Fischer, *Chem. Rev.* **2001**, *101*, 3581–3610; b) A. Goto, T. Fukuda, *Prog. Polym. Sci.* **2004**, *29*, 329–385.

[25] W. A. Braunecker, N. V. Tsarevsky, A. Gennaro, K. Matyjaszewski, *Macromolecules* **2009**, *42*, 6348–6360.

[26] W. Jakubowski, K. Min, K. Matyjaszewski, *Macromolecules* **2006**, *39*, 39–45.

[27] a) K. Matyjaszewski, H.-j. Paik, P. Zhou, S. J. Diamanti, *Macromolecules* **2001**, *34*, 5125–5131; b) J. Gromada, K. Matyjaszewski, *Macromolecules* **2002**, *35*, 6167–6173.

[28] M. Horn, K. Matyjaszewski, *Macromolecules* **2013**, *46*, 3350–3357.

[29] A. J. Niestroj, M. E. Maier, *Praxis in der Organischen Chemie*, VCH, Weinheim, **1997**.
[30] H.-D. Hardt, *Z. Anorg. Allg. Chem.* **1959**, *301*, 87–96.
[31] Bruker, in *SMART (Version 5.62), SAINT (Version 8.18 C, 2011), SHELXTL (Version 6.10), SADABS (Version V2012/1)*, Madison, Wisconsin, USA, **2002**.
[32] Bruker, in *XPREP*, Bruker AXS Inc., Madison, Wisconsin, USA, **2007**.
[33] G. Sheldrick, *Acta Crystallogr. Sect. A* **1990**, *46*, 467–473.
[34] C. B. Hübschle, G. M. Sheldrick, B. Dittrich, *J. Appl. Crystallogr.* **2011**, *44*, 1281–1284.

Manuscript received: December 14, 2020
Revised manuscript received: January 27, 2021
Accepted manuscript online: February 21, 2021

